Supporting Information

Ultrasensitive and Label-free Detection of Prognostic and Diagnostic Biomarker of Sepsis on AgNPs-laden Black Phosphorous based SERS Platform

Anirban Kundu, Renu Rani, Anas Ahmad, Ajay Kumar, Mamta Raturi, Tanya Gupta, Rehan Khan* and Kiran Shankar Hazra*

Institute of Nano Science and Technology, Knowledge City, Sector 81, Mohali,

Punjab, 140306, India

E-mail: kiran@inst.ac.in; rehankhan@inst.ac.in

Keywords: Sepsis; Surface enhanced Raman spectroscopy (SERS); Biomarker detection;

Layered black phosphorus (BP), spiked clinical sample.

1. Synthesis of AgNP@BP flake:
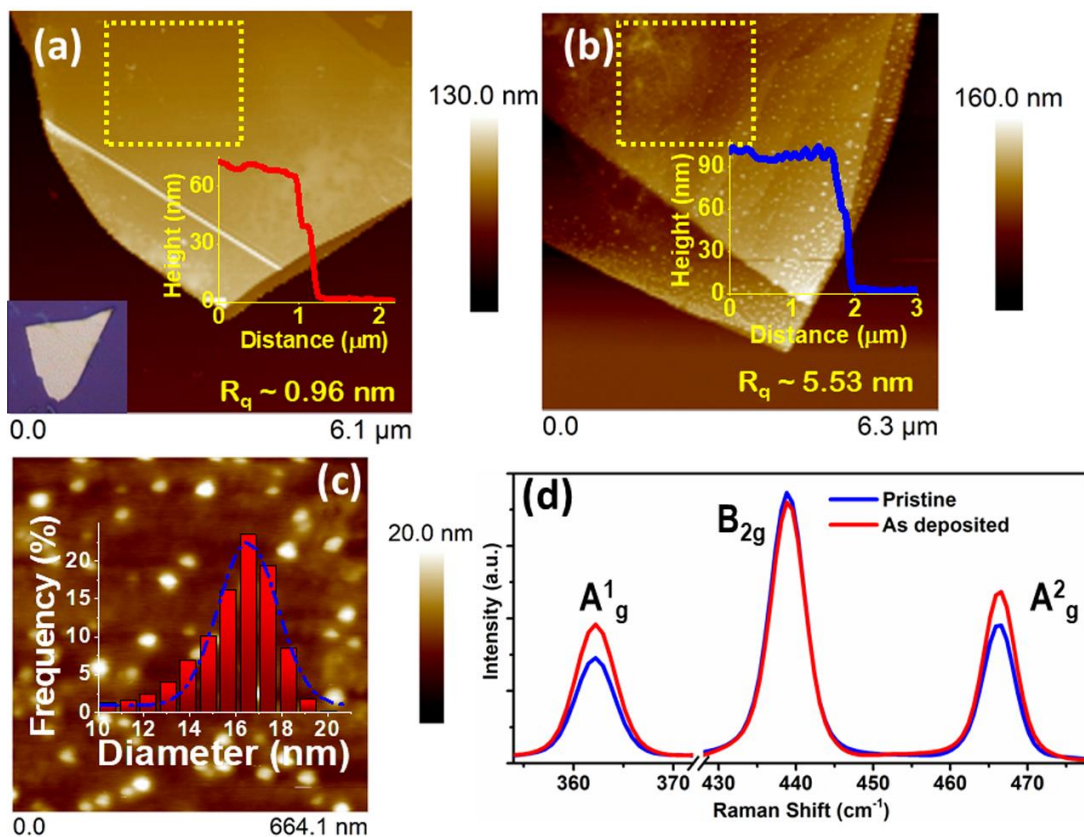
Figure S1| One-step synthesis of AgNPs decorated BP flake (AgNP@BP). (a) AFM height image of pristine BP flake with R_q ~ 0.96 nm, inset shows the optical image of the same flake; (b) AFM image of the AgNPs deposited BP flake with increased R_q ~ 5.53 nm; (c) The enlarged height image of AgNP@BP flake and the overlay plot shows the Gaussian particle size distribution having mean diameter of ~ 15.62±0.07 nm; and (d) Raman spectra of the pristine BP flake and AgNP@BP flake.

AFM topography image of pristine and AgNP@BP flakes are shown in Figure S1a-b, which suggests that the thickness of AgNP@BP flake (~ 91 nm) is increased by ~ 14 nm as compared to the pristine one (~ 77 nm). The height profile of the flakes has been shown in the overlay of Figure S1a-b, where the slight increase in thickness is observed due to deposition of AgNPs on the surface, defining the deposition process as a surface phenomenon and not due to the intercalation of the nanoparticles in between the BP nano-sheets/layers. Surface roughness of flakes, measured from the marked dotted area in Figure S1a-b, depict a six-fold enhancement in RMS (root mean square)

surface roughness (R_q) value of the AgNP@BP flake (Rq ~ 5.53 nm) as compared to the pristine one (Rq ~ 0.96 nm). The increase in surface roughness confirms the deposition of AgNPs exclusively on the surface of the BP flake, which forms the basis of AgNP@BP based SERS substrate. Enlarged topography image (Figure S1c) of the marked area shows that the as-grown AgNPs onto the surface of BP flake are distinct and uniformly distributed without any signature of agglomeration. The particle size distribution, shown in the histogram in the inset of Figure S1c, depicts that the deposited AgNPs have an average particle diameter of 16.52 ± 0.07 nm in a perfectly Gaussian distribution. The size and crystallinity of the nanoparticles has further been verified using transmission electron microscopy (TEM) imaging technique, as depicted in Figure S2-S4, where the optimization of the $AgNO_3$ concentration has also been described (Figure S4). Raman spectra of the pristine BP and AgNP@BP flakes are shown in Figure 1d, which shows three characteristics Raman modes A^1_g, $B_{2g,}$ and A^2_g, corresponding to out-of-plane vibration, in-plane vibration along zigzag and armchair direction, respectively. No significant shift in Raman peak position is observed for the characteristics Raman modes after adsorption of AgNPs on pristine BP flake, which confirms that the pristine structure of the BP flake remains unaltered and suggest that AgNPs are only adsorbed on the surface of the BP flake.

2. TEM characterization of AgNP@BP flake:
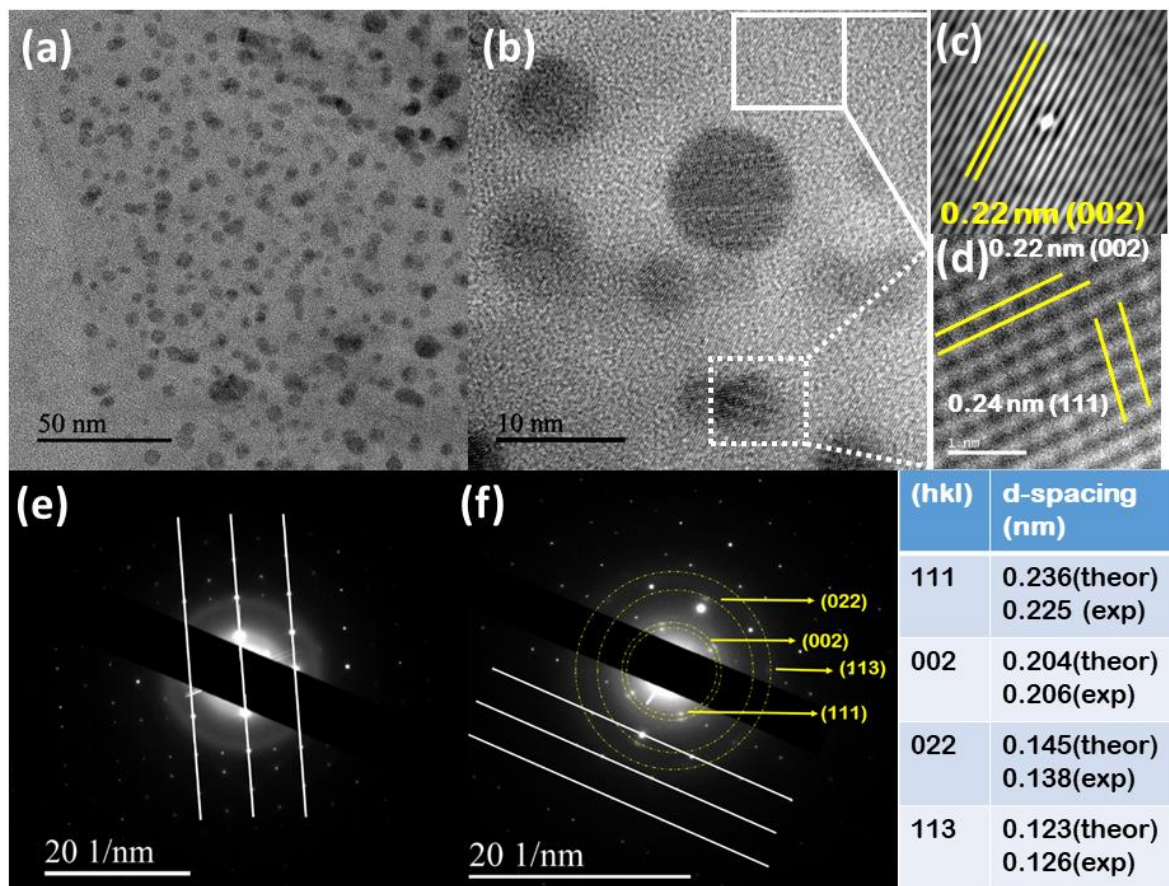
Figure S2| TEM analysis of the AgNP@BP flake. (a) TEM micrograph of as-deposited AgNP@BP flake with uniform distribution of the AgNPs over the surface of the BP flake; (b) HRTEM micrograph of the AgNP@BP flake showing the crystal planes of pristine BP and AgNP@BP flake; (c-d) Auto correlated FFT image of HRTEM micrograph of pristine BP flake and AgNPs@BP flake, respectively; (e-f) SAED pattern of pristine and AgNP@BP flake. The table shows the (hkl) planes AgNPs and their corresponding experimental and theoretical d-spacing value.

In order to investigate the size of the AgNPs and the crystalline nature of the flake, TEM analysis has been carried out for the pristine BP flake and AgNP@BP flake, as shown in Figure S2. The TEM micrograph of AgNP@BP flake (Figure S2a) confirms that the AgNPs are solely synthesized on the BP flake only, and no trace of AgNPs were found apart from the flake surface, which confirms that the BP flake assists the formation of AgNPs over its surface. The uniformly

distributed AgNPs, having average particle size distribution is found to be ~ 7.24 ± 0.18 nm, validate our previous analysis through AFM surface topography (Figure S2b). The inter particle distance has also been calculated, where the average distance has been found to be ~ 1.4 nm. Such small inter particle distance suggests that the AgNPs are well arranged and can have potential applications in terms of enhancement in localized electric field. The crystallinity of the AgNP@BP flake with area focused on BP (without AgNPs), and the area containing AgNPs are distinguished from the HRTEM images recorded by 200 KV electron microscope (Figure S2b). The d-spacing of the crystal planes corresponding to BP and AgNP are simulated from HRTEM micrographs using auto-correlated lattice fringe images. The comparison of the lattice fringes originated from the pristine area (solid box) and the AgNP deposited area (dotted box), are shown in Figure S2c and Figure S2d, respectively. The pristine area shows uniform lattice fringe of ~ 0.22 nm (Figure S2c) originating due to BP crystal corresponding to the (002) plane; whereas at the AgNP deposited area, the lattice fringes for both BP [of ~ 0.22 nm corresponds to (002) plane] and AgNPs [of 0.24 nm corresponds to (111) plane] are observed (Figure S2d). The selected area electron diffraction (SAED) pattern of pristine BP flake (Figure S2e) confirms its orthorhombic crystal structure, where bright spots corresponding to different planes, as marked in Figure S2f, are arranged in parallel lines (marked by white lines). The SAED pattern of the AgNP area (Figure S2f) confirms the highly crystalline nature of AgNPs, where the crystallinity of pristine BP flake remains unchanged. The characteristics crystal planes of the AgNPs, i.e., (111), (002), (022), and (113), are identified and indexed (with dotted circle in Figure S2f) in the SAED pattern of AgNP deposited area. The d-spacing (theoretical and measured) corresponding to that (hkl) crystal planes are tabulated in Table (Figure S2), where measured values match well with the theoretical value. The SAED pattern of AgNPs deposited area (Figure S2f), having diffraction patterns both from

BP flake and AgNP, confirms the strong adhesion of AgNPs on the BP surface. Qualitative

elemental analysis has also been carried out from the EDX techniques, as shown in Figure S3,

which confirms that no other elements apart from phosphorus and silver are present in the AgNP

deposited BP (AgNP@BP) flake.

3. <u>EDAX analysis of AgNP@BP flake:</u>
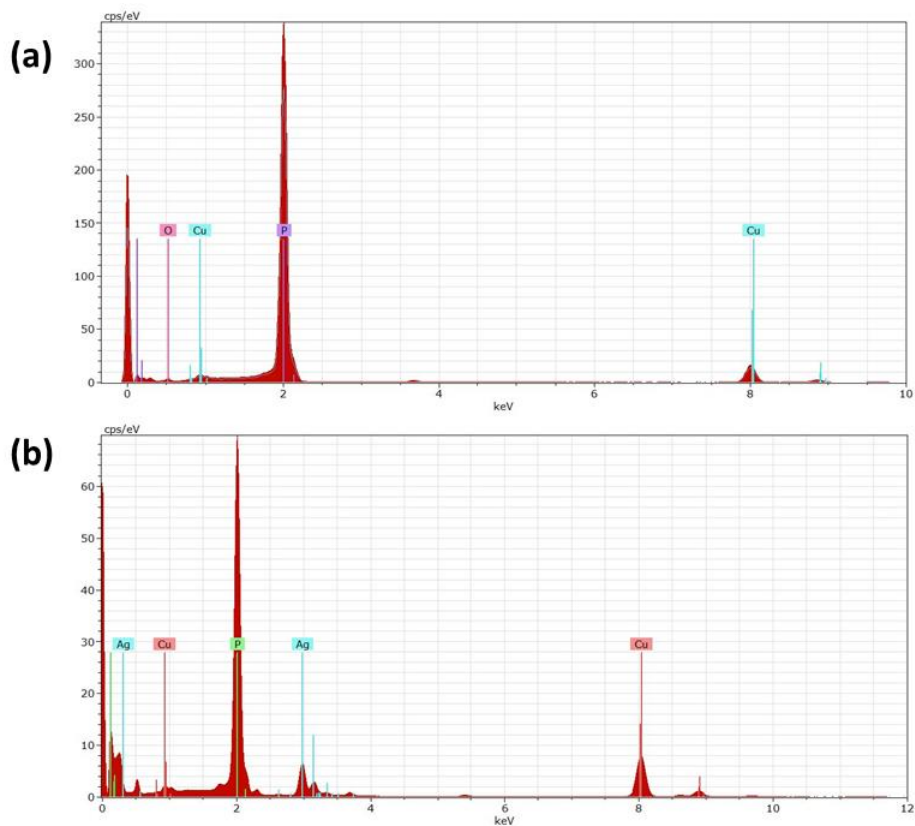
Figure S3| EDX spectra of (a) pristine BP flake and (b) AgNP@BP flake shows the presence of phosphorous in pristine BP and presence of both phosphorous as well as silver in AgNP@BP flake. The same flake has been used for EDX spectra analysis before and after the disposition of AgNPs. EDX spectra further shows that no oxidation of BP flake is occurred during AgNPs deposition.

4. Optimization of AgNO$_3$ concentration:
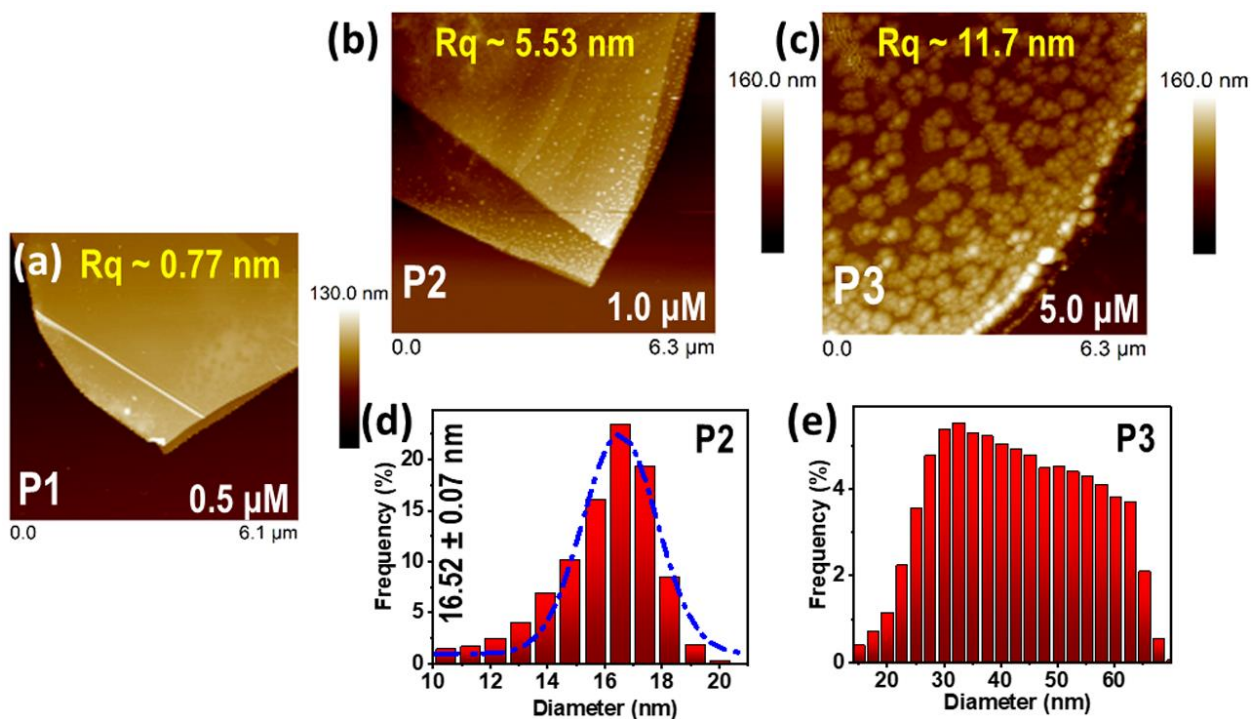
Figure S4| AFM height images and measured surface roughness of as deposited AgNP@BP flake, with the variation in concentration of AgNO$_3$ precursor solution of (a) 0.5 μM, (b) 1.0 μM and (c) 5.0 μM. The particle size distribution for the as deposited AgNP@BP flake correspond to the AgNO$_3$ concentration of (d) 1.0 μM and (e) 5.0 μM.

In order to control the particle size of the deposited AgNPs, the concentration of the precursor (AgNO$_3$) solution has been varied (P1: 0.5μM, P2: 1μM, and P3: 5μM) and simultaneously AFM height images of AgNP@BP flakes are recorded (Figure S4a-c). Though AgNPs are observed for P2 and P3 samples but no signature of nanoparticle deposition is found for sample P1. The particle size distribution (Figure S4d-e) is found to be quite uniform for the P2 sample. In contrast, agglomerated AgNPs are observed for the P3 sample (Figure S4c) and also exhibited non-uniform particle size distribution (Figure S4e). The surface roughness for all three samples is shown in Figure S4a-c, where it is evident that AgNPs deposition is uniform for sample P2, showing Gaussian distribution of particle size with mean value ~ 16.52 ± 0.07 nm, which are in good

7

agreement with the calculated average particle size distribution from TEM micrographs (Figure S2a). For sample P1, the surface roughness (Rq) is ~ 0.77 ± 0.002 nm, which is originating from the intrinsic roughness of the flake and similar to the RMS value of pristine BP flake (Rq ~ 0.96 nm), and hence no AgNP deposition is noticed. However, for sample P3, the surface roughness is ~ 11.7 nm, showing agglomeration of AgNPs with non-uniform particle size distribution, varying from 10 nm to 70 nm, confirming that further increase in the concentration of $AgNO_3$ in precursor solution leads to the agglomeration.

5. <u>Stability of AgNPs deposited BP flake (AgNP@BP):</u>
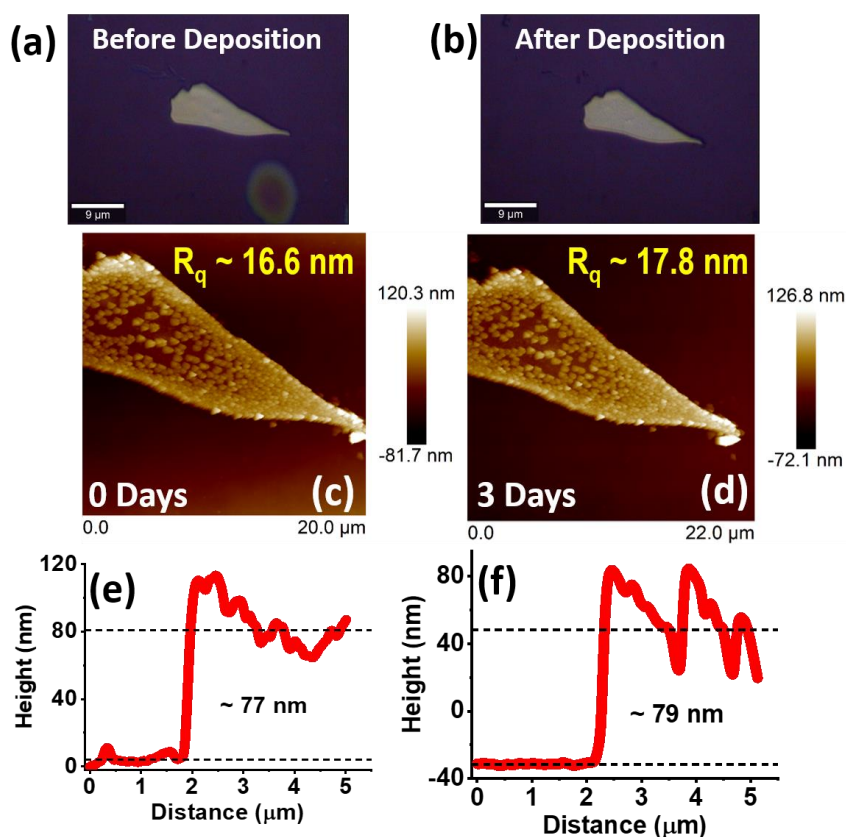
Figure S5| Optical image of BP flake (a) before and (b) after deposition of AgNPs. AFM height image and measured surface roughness (R_q) of the AgNP@BP flake after deposition at (c) 0 hrs and (d) 72 hrs or 3 days. Height profile at (d) 0 hrs and (e) 72 hrs confirms that no degradation in BP flake is observed.

6. <u>Raman spectra of LPS with different concentration of AgNO$_3$:</u>

Raman spectroscopy measurement has also been tried on different SERS substrate, where the concentration of AgNO$_3$ precursor has been varied. We have tried the SERS measurement on the substrate P1 and P3 with lipopolysaccharide (LPS) and corresponding Raman spectra are shown in Figure S6. Although the enhancement in Raman signal is observed for both P1 and P3, but the Raman modes are not distinguishable as compare to the Raman signal observed for P2. Thus, it can be concluded that the uniform distribution of AgNPs is an essential factor for appropriate Raman signal. For substrate P3, the agglomeration of AgNPs is the key reason for ineffective Raman spectra. Hence, all the Raman enhancement experiments for IL-3 and PCT are performed on a similar substrate as P2, where the initial concentration of aqueous AgNO$_3$ is 1 μM.
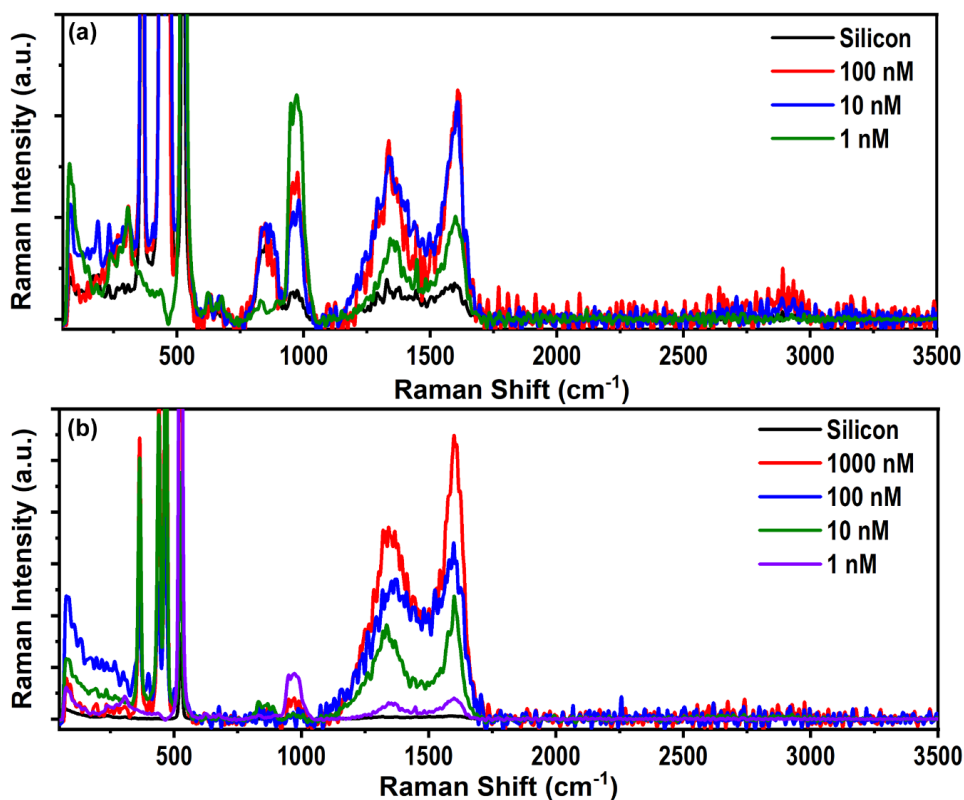
Figure S6| Raman spectra of LPS with varying concentration upto 1 nM on different AgNP@BP substrate where precursor AgNO$_3$ concentration are (a) 0.5 μM and (b) 5.0 μM.

7. Identification of hotspot area at AgNP@BP flake:

In order to calculate the number of particles present in a particular area, we have chosen seven (7) different areas ranging from ~ 0.44 μm^2 to ~ 4.0 μm^2 and identified the particles from the AFM analysis to calculate the number of silver nanoparticles (AgNPs). The AFM height and phase images of the seven different regions are shown in Figure S7, where each area has been named as A, B, C, D, E, F and G. To calculate the number of AgNPs, we have used the phase images as the contrasts in nanoparticles are clearly visible in the phase images as compared to the height images. The table ST1 shows the calculated area of different region, number of particles in that area and per unit area. From the table we have calculated the average number of particles per unit area, which has further been used to calculate the SERS enhancement factor (EF).
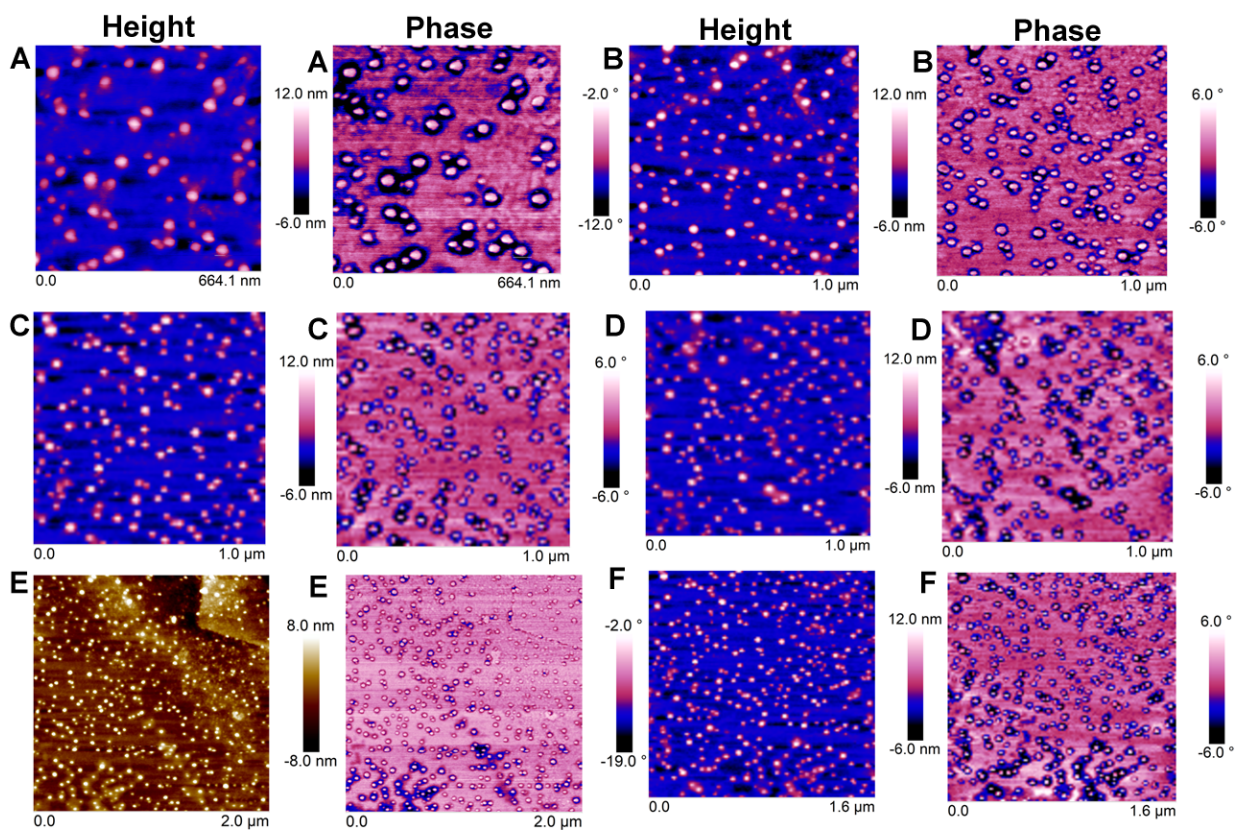
Figure S7| The AFM height and phase image of six different regions (A-F), where the phase images give better contrast of the AgNPs present on the SERS substrate.

Table ST1: *Tables shows the dimension, area (A), number of particles (N) and corresponding average number of particles per unit area (n).*

	A	B	C	D	E	F
Horizontal Dimension (µm)	0.66	1.0	1.0	1.0	2.0	1.6
Vertical Dimension (µm)	0.66	1.0	1.0	1.0	2.0	1.6
Area (A) (µm^2)	~ 0.44	1.0	1.0	1.0	4.0	2.56
No. of Particles (N)	65	175	122	145	451	302
No. of Particles/µm^2 (n)	~149	~175	~122	~145	~113	~118
Average No. of Particles/µm^2 (N$_{av}$)	~141					

8. <u>Identification of hotspot area under laser illumination:</u>

The SERS enhancement factor depends on the number of AgNPs present on the surface under the laser illumination, as the target molecules attached to the AgNPs, only contribute to the SERS signal.[1] Thus, the total area contributing to the SERS signal will be $A_{SERS} = N_{Av} \times \pi d_n^2/4 \times A_{Normal}$, where N_{Av} is the average number of AgNPs per unit area, d_n is the mean diameter of the AgNPs and A_{Normal} is the laser illuminated area. The laser illuminated area (A_{Normal}) has been calculated from the diameter of the laser beam, which is measured by analyzing the Gaussian beam profile of the laser beam by acquiring the optical image of the laser spots. Such measurement shows that the diameter of the laser beam is ~0.995 µm, which is considered as $d \sim 1$ µm for further calculations of $A_{Normal} = \pi d^2/4 = \pi (1)^2/4 \ \mu m^2 = 0.785 \ \mu m^2$. Whereas, the A_{SERS} has been calculated from the covered area of the AgNPs under the laser illuminated area as $A_{SERS} = N_{Av} \times \pi d_n^2/4 \times$

A_{Normal}, which lead to $A_{SERS} = 141 \ x \ \pi d_n^2/4 \ x \ 0.785 \ \mu m^2 = 141 \ x \ \pi \ (0.01652)^2/4 \ x \ 0.785 \ \mu m^2 =$

$0.00755 \ \mu m^2$. Such value suggests that the A_{SERS} is 2-order smaller as compare to the A_{Normal}.

9. <u>Calculation of laser beam diameter</u>
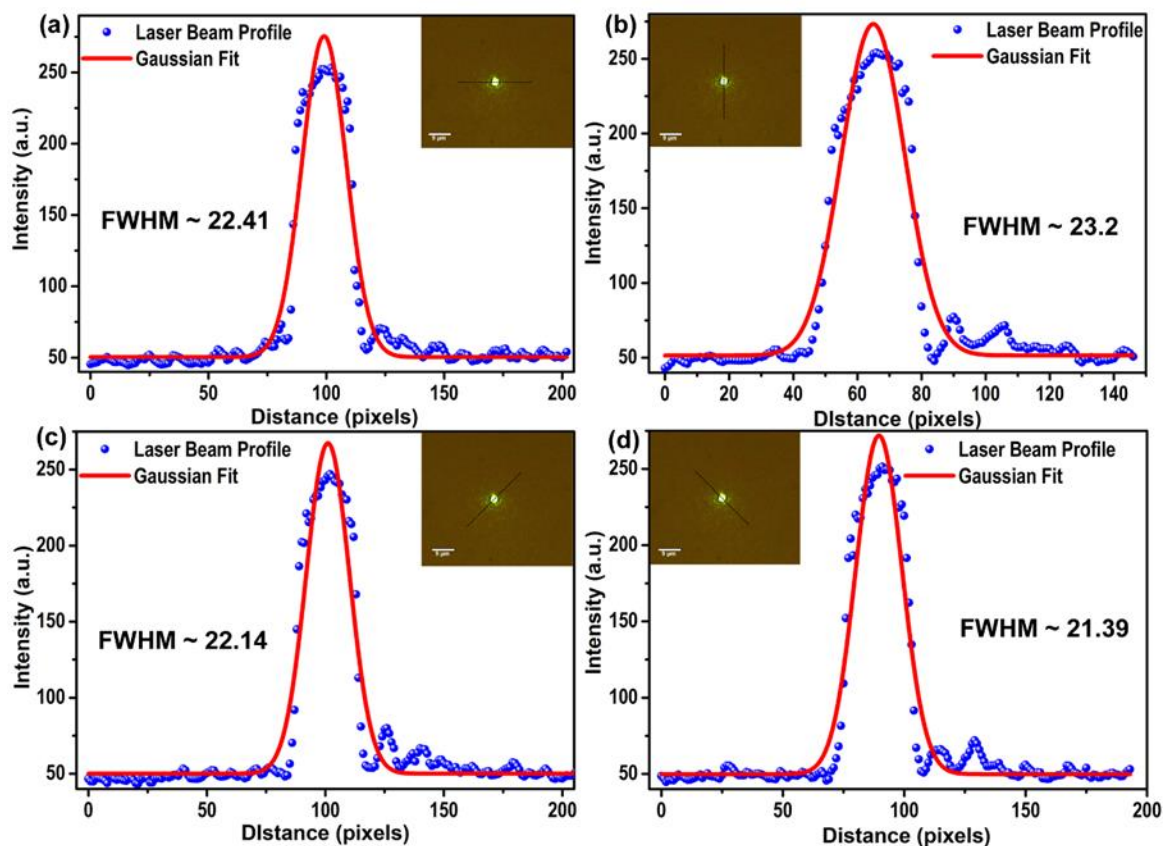
Figure S8| Laser beam intensity profile to calculate the beam diameter. Inset shows the reflected optical image of the beam intensity focused using 100X objective. The beam profile has been extracted along directions shown by black likes in the optical images. Average FWHM ~ 22.12 pixels, which corresponds to ~ 0.995 μm. The figure is reproduced from Ref. 11 with permission from the Royal Society of Chemistry.

10. Details of calculation of SERS enhancement factor (EF):

To estimate the SERS enhancement factor (EF) of the probe molecule in the hotspot region, the following equation has been employed $EF = (I_{SERS} \times N_{Normal})/(I_{Normal} \times N_{SERS})$, where I_{SERS} and I_{Normal} are the intensities of the same Raman mode for the SERS and normal Raman spectra, N_{Normal} is the number of molecules probes for a normal Raman scattering and N_{SERS} is the number of molecules probed in SERS.[1,2] The areas of the Raman bands are used as the intensities of I_{SERS} and I_{Normal}. The number of probe molecules in normal Raman scattering can be estimated from the laser illuminated area (A_{Normal}), where the area can be calculated from the laser spot size. Here, all the molecules present in that area contribute to the intensities of the normal Raman signal (I_{Normal}), whereas the molecules only present in the hotspot area contribute to the SERS Raman signal (I_{SERS}). This fact leads to the modification of the equation and the simplified equation becomes $EF = (I_{SERS} \times A_{Normal})/(I_{Normal} \times A_{SERS})$, where A_{Normal} is the laser illuminated area and A_{SERS} is the total area of hotspots under the laser illuminated area.

11. Single Raman spectra of IL-3 and PCT
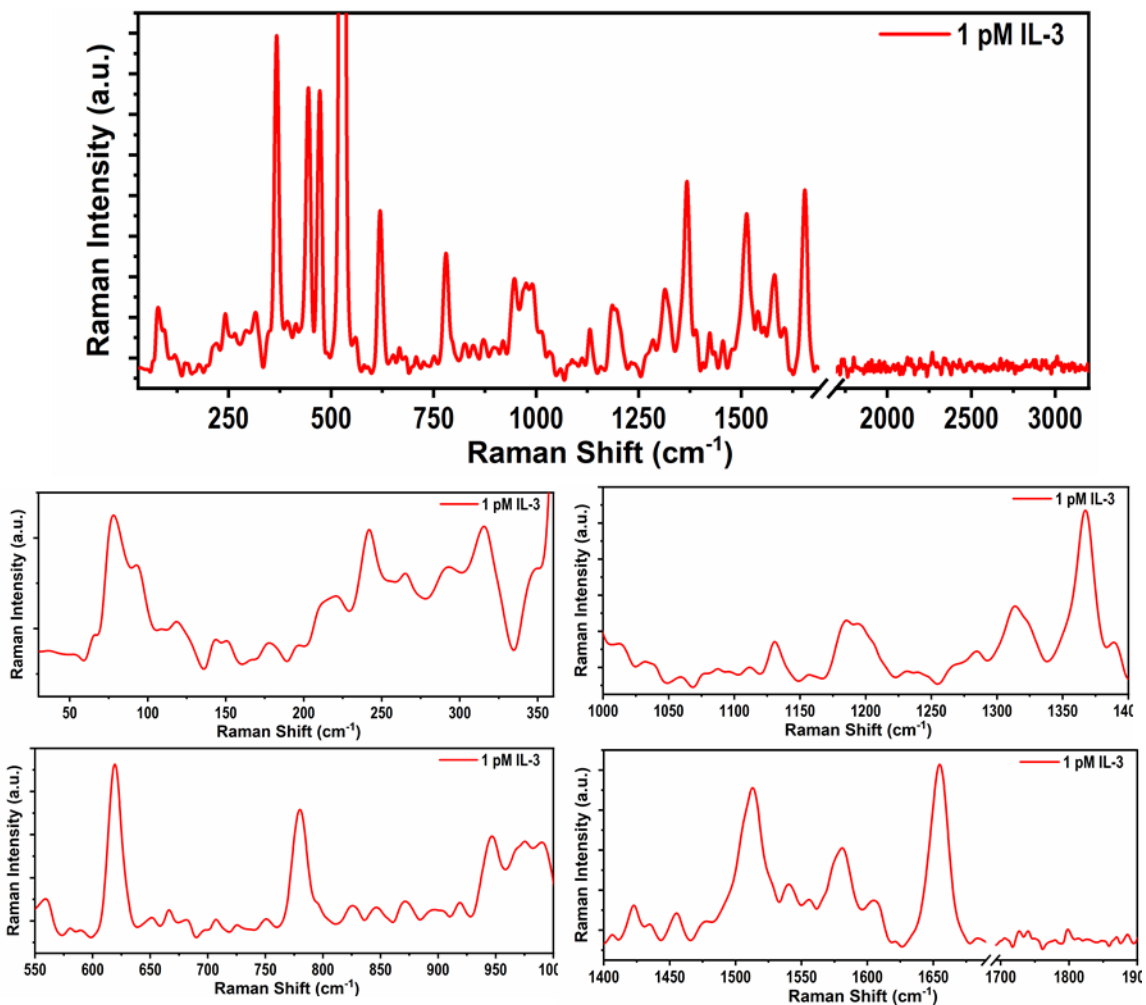
Figure S9| Raman spectra of IL-3 biomarker, where the range of Raman spectra is zoomed into four different regions as 50-360 cm^{-1}, 550-1000 cm^{-1}, 1000-1400 cm^{-1} and 1400-1900 cm^{-1}.
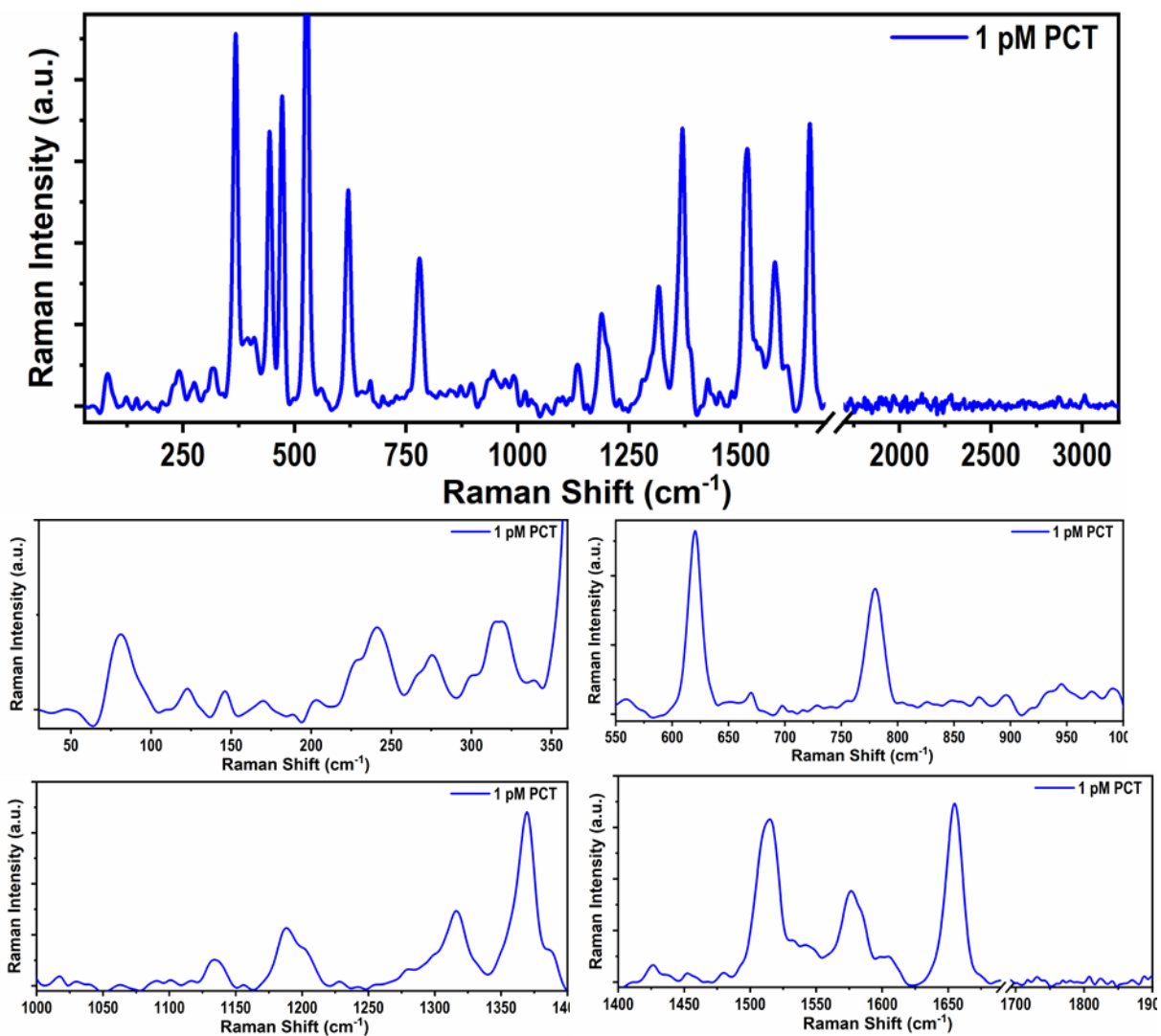
Figure S10| Raman spectra of PCT biomarker, where the range of Raman spectra is zoomed into four different regions as 50-360 cm^{-1}, 550-1000 cm^{-1}, 1000-1400 cm^{-1} and 1400-1900 cm^{-1}.

12. Statistical Analysis of Raman intensity fluctuation
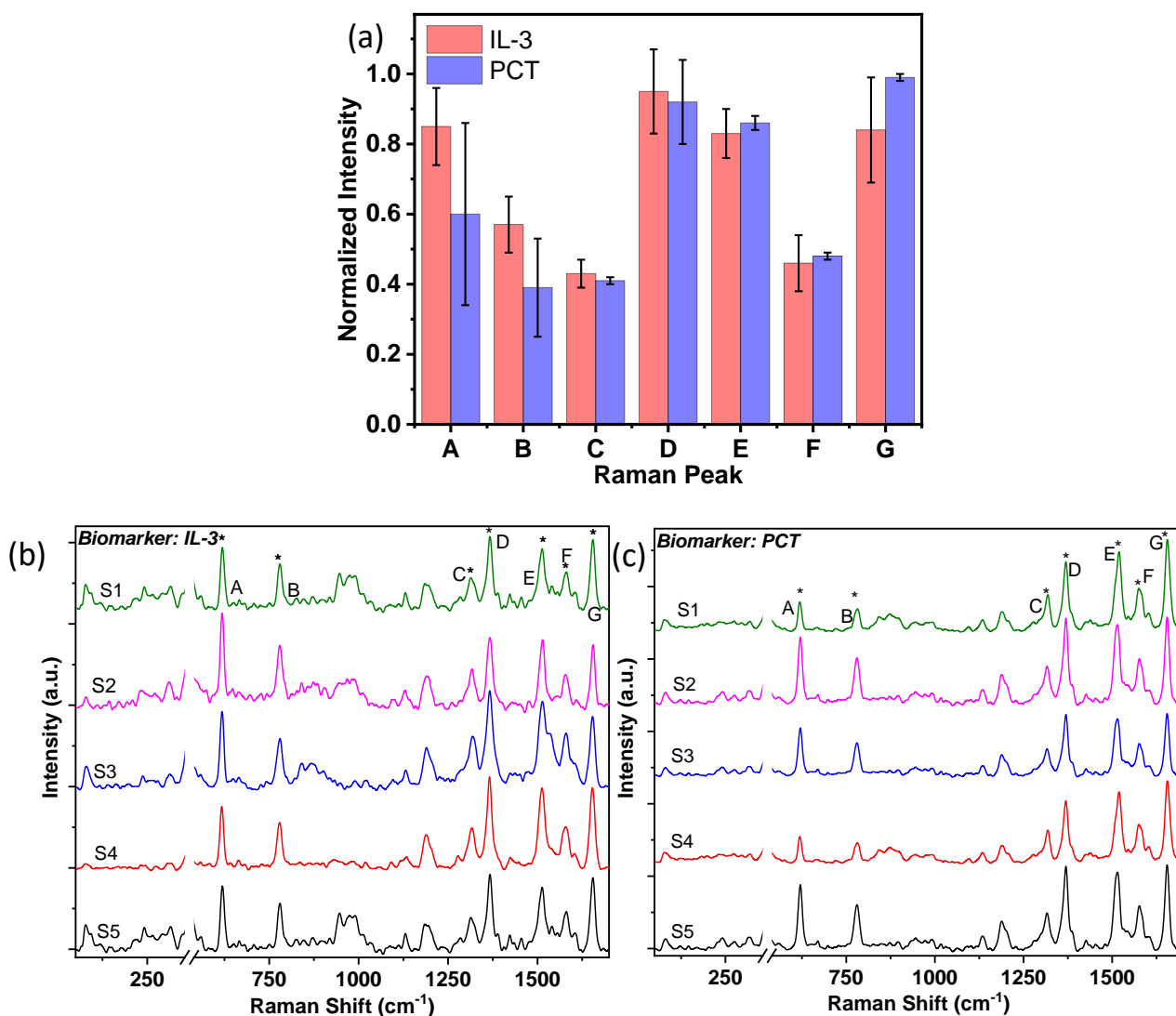
Figure S11| (a) Fluctuation of Raman intensity for the different Raman peaks. The Raman spectra of the (b) IL-3 and (c) PCT biomarkers recorded from five different samples, where the mean Raman intensity fluctuation is found to be ~ 0.094 and ~ 0.08 for IL-3 and PCT, respectively.

In order to find the intensity fluctuation on the Raman peaks, we have normalized each spectrum with respect to the highest intense peak and calculated the standard deviation of the peak intensity for the six high intense peaks for both the biomarkers. The statistical analysis of the Raman spectra has been done based on the collected spectra from different samples, where each spectrum has been presented after averaging out multiple acquisitions of Raman spectra. For each concentration

of a particular biomarker, 5 samples were prepared and tested to check the reproducibility; likewise, 5 different concentrations are tested for a particular biomarker. Each presented spectrum in the manuscript is averaged from 10 separate spectra collected with acquisition time ~ 30 sec each. Such averaging of the spectra is done to increase the signal to noise ratio of the spectra. Figure S11 depicts the Raman spectra in the revised SI for both the biomarkers (IL-3 & PCT) for five different samples of same concentration (~1000 pM) to show the intensity fluctuation in the Raman spectra. The as calculated standard deviation is demonstrated in the following Table ST2, where the mean standard deviation for IL-3 and PCT are found to be ~0.094 (error ~ ±9.4%) and ~0.080 (error~ ±8%), respectively; which significantly low and indicates excellent reproducibility.

Table ST2: *Intensity fluctuation of Raman peaks of IL-3 and PCT*

Peak Position	IL-3	PCT
A. 621.04	0.111	0.268
B. 782.35	0.080	0.141
C. 1319.56	0.041	0.007
D. 1369.34	0.123	0.116
E. 1520.92	0.074	0.014
F. 1573.51	0.088	0.014
G. 1653.75	0.147	0.005
Average Intensity Standard Deviation	0.094	0.080

13. Raman spectra of Si_BP, Si_Buffer and Si_AgNP@BP_Buffer
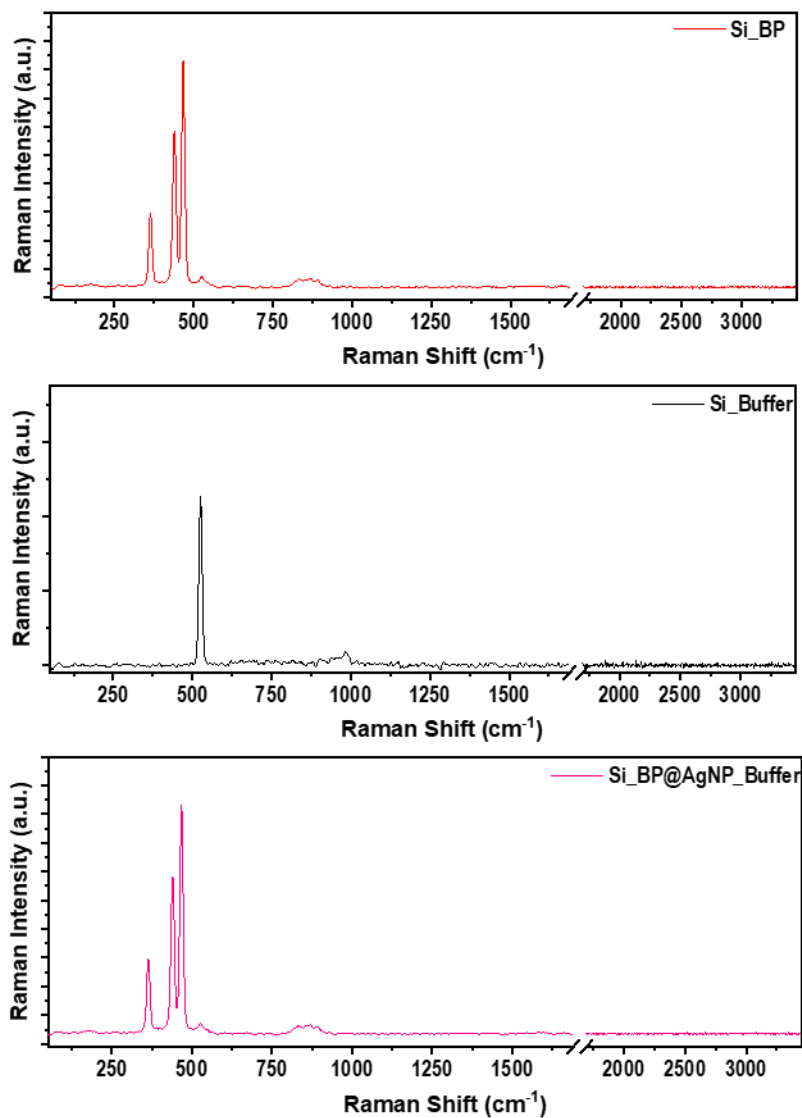
Figure S12| Raman spectra of the reference level from Si_BP, Si_Buffer and Si_AgNP@BP_Buffer.

Table ST3: *Raman peak position and corresponding band assignment of lipopolysaccharide (LPS).*[3,4]

Raman Peak Position (cm^{-1})	Band Assignment	Origin of Raman bands
620	Bending of COO	
777	C-C stretching	Highly mixed in complex molecule (Alicyclic molecules)
1131	C-O-C group stretching C-C stretching	Presence of lipid Due to polyethylene group
1194	-	Unidentified
1316	C-C bending	Aliphatic molecules
1366	CH$_3$ bending	Lipids
1534	C-C stretching	Aromatic ring vibration (mild)
1579	C-C stretching	Presence of Graphitic carbon
1655	C=C stretching C=N stretching ,	Lipids Lipids
2900	C=O stretching CH$_3$ stretching	Sugar Presence of lipid Presence of polyethylene group

14. Estimation of SERS EF of lipopolysaccharide (LPS):

The SERS EF of LPS has been calculated from the two strongest Raman bands at 1366 and 1655 cm^{-1} for three different concentrations of 1000 nM, 100 nM and 1 nM. Here, the SERS intensities and corresponding SERS enhancement factors are tabulated in Table ST3.

Table ST4: *SERS EF of lipopolysaccharide (LPS) for Raman peaks at 1366 and 1655cm^{-1} with the variation in LPS concentration.*

LPS	1366 cm^{-1}	1655 cm^{-1}
	SERS EF	
1000 nM	5.47 x 10^{14}	0.83 x 10^{14}
100 nM	3.18 x 10^{14}	3.2 x 10^{14}
1 nM	1.56 x 10^{14}	3.2 x 10^{14}
Mean SERS EF	2.9 x 10^{14}	
Limit of Detection (LOD)	1 nM	

15. Estimation of SERS EF of interleukin-3 (IL-3):

The SERS EF of IL-3 has been calculated from the three strongest Raman bands at 620, 1366 and 1655 cm^{-1} for four different concentrations of 1000 pM, 100 pM, 10 pM and 1 pM. Here, the SERS intensities and corresponding SERS enhancement factors are tabulated in Table ST4.

Table ST5: *SERS EF of interleukin-3 (IL-3) for Raman peaks at 620, 1366 and 1655cm^{-1} with the variation in IL-3 concentration.*

IL-3	620 cm^{-1}	1366 cm^{-1}	1655 cm^{-1}
	SERS EF		
1000 pM	2.9×10^{14}	3.37×10^{13}	3.91×10^{14}
100 pM	1.2×10^{14}	1.91×10^{14}	2.57×10^{14}
10 pM	1.49×10^{14}	2.66×10^{14}	3.86×10^{14}
1 pM	1.11×10^{14}	1.5×10^{14}	1.13×10^{14}
Mean SERS EF	2.3×10^{14}		
Limit of Detection (LOD)	1 pM		

16. Estimation of SERS EF of procalcitonin (PCT):

The SERS EF of PCT has been calculated from the three strongest Raman bands at 620, 1366 and 1655 cm^{-1} for two different concentrations of 1000 fM and 100 fM. Here, the SERS intensities and corresponding SERS enhancement factors are tabulated in Table ST5.

Table ST6: *SERS EF of procalcitonin (PCT) for Raman peaks at 620, 1366 and 1655cm^{-1} with the variation in PCT concentration.*

PCT	620 cm^{-1}	1366 cm^{-1}	1655 cm^{-1}
	SERS EF		
1000 fM	6.49 x 10^{14}	8.0 x 10^{14}	9.4 x 10^{14}
100 fM	1.53 x 10^{14}	4.29 x 10^{14}	6.26 x 10^{14}
Mean SERS EF	4.49 x 10^{14}		
Limit of Detection (LOD)	100 fM		

Table ST7: *Summary of the obtained SERS enhancement factor (EF) and limit of detection (LOD) values for different biomarkers.*

Biomarkers	LPS	IL-3	PCT
EF	2.9 x 10^{14}	2.3 x 10^{14}	4.5 x 10^{14}
Limit of Detection	1 nM	1 pM	100 fM

Table ST8: *Raman fingerprint modes of IL-3 and PCT.*

Biomarkers	Wavenumber (cm⁻¹)
IL-3	65, 92, 118, 177, 221, 265, 292, 347, 579, 681, 702, 919, 1111, 1285, 1406, 1739, 1752, 1798
PCT	122, 170, 229, 203, 299, 740, 803, 1100, 1228, 1254, 1692, 1807, 1824, 1841, 1888

Table ST9: *Raman peak positions of IL-3 & PCT in clinical sample and confirmation with respect to the observed peak for pure biomarkers.*

Serum + IL-3	Observed for Pure IL-3	Serum + PCT	Observed for Pure PCT
129.45	YES	116.01	YES
146.57	YES	139.51	YES
409.52	YES	171.93	YES
801.95	YES	196.38	YES
834.32	YES	219.77	YES
869.78	YES	244.86	YES
892.89	YES	974.1	YES
1178.35	YES	1044.02	YES
1298.17	YES	1084.62	YES
1364.3	YES	1128.32	YES
1372.58	YES	1280.5	YES
1421.57	YES	1316.83	YES
1518.44	YES	1361.54	YES
1552.5	YES	1373.38	YES

1569.84	YES	1437.69	YES
1648.54	YES	1516.61	YES
		1547.14	YES
		1572.83	YES
		1607.63	YES
		1655.59	YES

Table ST10: *Raman peak positions, band assignment, and origin of Raman modes for human serum and mixed (IL-3 + PCT) clinical sample.*[5–10]

Human Serum	Origin	Serum + IL-3 + PCT	Origin
856.21	Proline, hydroxyproline, and tyrosine C-C stretching	114.56	IL-3
893.02	Tryptophan, δ (ring)	122.31	PCT
934.48	C-C stretch of proline ring/glucose/lactic acid; C-C, praline ring (collagen assignment)	135.76	IL-3
943.17		146.36	IL-3, PCT
956.22	Hydroxyapatite, carotenoid, and cholesterol	194.28	IL-3
1132.89	the strong C-O band of ribose	221.16	IL-3
1175.58	(CH) phenylalanine, tyrosine	228.07	PCT
1215.08	C-C6H5 stretching mode in tyrosine and phenylalanine	268.21	IL-3
1255.44	Lipids	412.48	IL-3
1265.73	Symmetric Ring deformation; tyrosine	437.43	IL-3, PCT
1276.9	Typical phospholipids, C=C groups in fatty acids, amide III band in proteins	464.95	IL-3, PCT
1314.46	G ring breathing modes of the DNA/RNA	472.04	IL-3, PCT
1335.47	Polynucleotide chain (DNA purine bases)	614.48	
1345.73	C-H bending; Tryptophane	617.53	IL-3, PCT
1376.64	δCH3 symmetric (lipid assignment)	632.82	IL-3
1408.34	CH2, CH3 bending; phosphatase	668.58	IL-3, PCT
1423.81	G, A (DNA, RNA)	714.64	IL-3
1446.8	CH2 bending mode of proteins and lipids	811.17	PCT
1458.82	δCH2, disaccharides	833.92	IL-3
1480.42	Guanine (N7)	861.89	Serum, IL-3

1531.75	Amide carbonyl group vibrations and aromatic hydrogens	883.17	IL-3
1558.53	Tryptophan	914.47	IL-3
1583.62	δ(C-C), phenylalanine	987.3	IL-3, PCT
1643.91	Amide I band (protein band)	1077.5	PCT
1681.67	Amide I	1128.2	IL-3
2907.08	CH asymmetric Stretching; Dimethylthio-acetamide	1175.77	Serum
2915.17	CH band of lipids and proteins	1194.2	IL-3
2968.12	CH2 asymmetric Vibration; L-asparagine	1239.24	PCT
		1253.19	Serum
		1259.17	PCT
		1293.62	IL-3
		1334.09	Serum
		1350.36	Serum
		1360.36	IL-3
		1375.45	Serum, IL-3, PCT
		1409.94	IL-3
		1420.98	IL-3, PCT
		1435.48	IL-3, PCT
		1441.96	Serum
		1479.64	Serum, IL-3
		1513.68	IL-3, PCT
		1534.18	Serum
		1554.96	IL-3, PCT
		1574.06	IL-3, PCT
		1583.5	Serum
		1648.35	Serum
		1659.68	IL-3, PCT
		1680.51	Serum
		1688.5	PCT
		1743.02	IL-3

References:

(1) Lin, D., Wu, Z., Li, S., Zhao, W., Ma, C., Wang, J., ... & Yang, X. **2017**. ACS nano, 11(2), 1478-1487.

(2) Erridge, C., Bennett-Guerrero, E. & Poxton, I. R. Structure and function of lipopolysaccharides. Microbes Infect. 4, 837–51 (2002).

(3) Trueblood, J. V., Estillore, A. D., Lee, C., Dowling, J. A., Prather, K. A., & Grassian, V. H. The Journal of Physical Chemistry A, 120(32), 6444-6450 (2016).

(4) Cochran, R. E., Laskina, O., Trueblood, J. V., Estillore, A. D., Morris, H. S., Jayarathne, T., ... & Laskin, A. *Chem*, 2(5), 655-667 (2017).

(5) Kotanen, C. N.; Martinez, L.; Alvarez, R.; Simecek, J. W. *Bio-Sensing Res.* **2016**, *8*, 20–26.

(6) Ma, H.; Sun, X.; Chen, L.; Han, X. X.; Zhao, B.; Lu, H.; He, C. *Anal. Chem.* **2018**, *90* (21), 12342–12346.

(7) Sahu, A.; Sawant, S.; Talathi-Desai, S.; Murali Krishna, C. *Biomed. Spectrosc. Imaging* **2015**, *4* (2), 171–187.

(8) Atkins, C. G.; Buckley, K.; Blades, M. W.; Turner, R. F. B. *Appl. Spectrosc.* **2017**, *71* (5), 767–793.

(9) Zou, Y.; Xia, P.; Yang, F.; Cao, F.; Ma, K.; Mi, Z.; Huang, X.; Cai, N.; Jiang, B.; Zhao, X.; et al. *Anal. Methods* **2016**, *8* (18), 3763–3767.

(10) Fenn, M. B.; Xanthopoulos, P.; Pyrgiotakis, G.; Grobmyer, S. R.; Pardalos, P. M.; Hench, L. L. *Adv. Opt. Technol.* **2011**, *2011*.

(11) Kundu, A.; Rani, R.; Hazra, S. K. *Nanoscale*, **2019**,11, 16245-16252